Vibrational Circular Dichroism of 1,1′-Binaphthyl Derivatives: Experimental and Theoretical Study

Vladimír Setnička,[†] Marie Urbanová,[‡] Petr Bouř,*,[†,§] Vladimír Král,[†] and Karel Volka[†]

Departments of Analytical Chemistry and of Physics and Measurement, Institute of Chemical Technology, Technická 5, 166 28 Praha 6, Czech Republic, and Institute of Organic Chemistry and Biochemistry, Academy of Sciences of the Czech Republic, Flemingovo nám. 2, 16610, Praha 6, Czech Republic

Absorption and vibrational circular dichroism (VCD) spectra of six 1,1′-binaphthyl derivatives were measured and analyzed on the basis of ab initio modeling. The spectra of both enantiomers were recorded with a high signal-to-noise ratio. The BPW91/6-31G** density functional theory level and the gauge invariant atomic orbitals were used for the simulations of VCD intensities. The binaphthyl moiety behaves as a chiral chromophore with a strong VCD signal because the 1,1′-substitution hinders its rotation. Most of the VCD bands were assigned, and the contributions of the binaphthyl skeleton and the functional groups could be clearly distinguished. Distinct VCD characteristics were found for the compounds exhibiting C_2 and C_1 symmetry. A very good agreement between the calculated and experimental spectra was observed. Apart from indication of enantiomeric purity, the spectra contain readable information about molecular conformation. The dihedral angle between the naphthyls planes, equal to about 55° when naphthyl residues were connected with PO_4 covalent bridge, was found close to 90° for all the other derivatives.

Introduction

1,1′-Binaphthyls represent popular building blocks for construction of chiral recognition receptors and chiral catalysts.[1] Whereas fast racemization for the plain 1,1′-binaphthyl was reported, the hindrance of its rotation after a 2,2′-substitution makes chiral conformers stable[2] and they therefore can be used as true enantiomers. Moreover, such systems exhibit outstanding chiral recognition as specific receptors[1a] and enantioselective separators.[3] They were also applied for construction of enantioselective catalytic systems and used as a vital part of the asymmetric ligands in complexation of palladium(II), rhodium-(II) and ruthenium (II), and titanium(IV) ions.[4]

Detailed information about conformation of the 1,1′-binaphthyl derivatives in the crystalline state can be obtained from X-ray crystallography.[5] Solution structures were analyzed by a variety of spectroscopic methods.[4d,6] A relatively tight correlation between the spatial arrangement and spectral signal was found namely for the electronic (ECD)[6a−e] and vibrational circular dichroism (VCD)[6f] techniques. Stereochemical parameters of binaphthyls were also studied by an analysis of the twisting power of nematic liquid crystals.[7] The angle θ defining the deviation of the two naphthyl planes plays an important role in the discriminating ability of 1,1′-binaphthyls in the enantiomeric reactions and chiral recognition.[8] According to its value transoid ($\theta > 90°$) or cisoid ($\theta < 90°$) forms of the binaphthyls were distinguished.[2] Two crystalline forms of nonsubstituted 1,1′-binaphthyl with $\theta = 103°$ and $\theta = 98.8°$ were reported by the X-ray studies.[5] Values of θ for several derivatives in solution were obtained by using a wavelength splitting of the 220 nm

couplet in the ECD spectra.[6a−f,9] Computational study of the rotation about the pivotal bond connecting the naphthyl moieties was performed.[9]

However, detailed information about the molecular conformation in solution cannot be usually obtained from ECD studies because of the sensitivity of the signal to molecular environment, band overlapping, small number of the electronic transitions, and a lack of accurate theoretical models for spectral interpretation. Thus, it seems convenient to use the additional information from the measurement of VCD[10] spectra, which provide better resolution and reveal finer details about molecular structure. Previous VCD study of binaphthyls[6f] dealt with the OH stretching vibrations. Because these are affected by the hydrogen bonding and anharmonic interactions, information about the arrangement of the binaphthyl core cannot be easily extracted. Furthermore, the semiempirical dipolar model used in the study was inadequate for VCD interpretation.[10e]

Here we present VCD spectra in the mid-IR region of a series of binaphthyl derivatives of a common structure,

(S)-enantiomer　　　(R)-enantiomer,
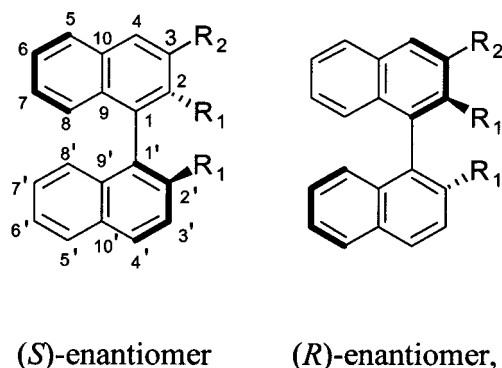
and compare them with simulations based on ab initio calculations. This method, as shown below, allows us to monitor not

---

* To whom correspondence should be addressed. E-mail: bour@uochb.cas.cz.
† Department of Analytical Chemistry, Institute of Chemical Techology.
‡ Department of Physics and Measurement, Institute of Chemical Technology.
§ Academy of Sciences of the Czech Republic.

TABLE 1: List of the Binaphthyl Derivatives

compound	R_1	R_2
1	H	H
2	OH	H
3	NH2	H
4	OSO_2CF_3	H
5	OH	COOH
6	OH	$COOCH_3$
7	PO_4H (bridge between both positions R_1)	H

only the absolute chirality of the molecules, but also individual contributions of the functional groups to the spectra and molecular conformations. As follows from theoretical considerations the contribution of the primary 1,1′-binaphthyl core can be clearly distinguished for the set of model compounds, thus making the interpretation easier. The parent binaphthyl system **1** (see Table 1) exhibits a fast racemization (in minutes) and its VCD spectra thus cannot be obtained with available spectrometers. On the other hand, 2,2′-dihydroxy- (**2**), 2,2′-diamine- (**3**), 2,2′-bis(trifluoromethanesulfonate)- (**4**), 2,2′-dihydroxy-3-carboxy- (**5**), 2,2′-dihydroxy-3-methoxycarbonyl- (**6**), and a cyclic phosphodiester (**7**) derivatives of 1,1′-binaphthyl are stable, and their racemization is not observed at the room temperature. A general aim of this article is to obtain more experimental and theoretical knowledge about substituted binaphthyl derivatives and about influence of different functionalities on detailed geometry and subsequently enantioselective induction. Additionally, we want to explore the potential of the VCD spectroscopy as one of the few techniques that reflect the detailed structure of individual molecules in solution.

Experiment

Six derivatives **2**−**7** both in the (S)- and (R)-enantiomeric forms (Table 1) were used for the collection of VCD spectra. (S)-(−)- and (R)-(+)-1,1′-binaphthyl-2,2′-diol, 99% (**2**), was purchased from Merck (814773, 814774). (S)-(−)- and (R)-(+)-1,1′-binaphthyl-2,2′-diamine, 99% (**3**), and (S)-(+)- and (R)-(−)-1,1′-bi-2-naphthol bis(trifluoromethanesulfonate), 97% (**4**), were purchased from Aldrich (38,243-4; 38,242-6; 43,189-3; 44,059-0). (S)-(−)- and (R)-(+)-1,1′-binaphthyl-2,2′-diol-3-carboxylic acid (**5**) and (S)-(−)- and (R)-(+)-1,1′-binaphthyl-2,2′-diol-3-methyl carboxylate (**6**) were prepared in purity higher than 98% in our laboratory.[11] (S)-(+)- and (R)-(−)-1,1′-binaphthyl-2,2′-diyl hydrogenphosphate, 98% (**7**), were purchased from Fluka (14375) and Aldrich (24,893-2), respectively. All the samples were studied without further purification as solutions in deuterated dimethyl sulfoxide DMSO-d_6 (Chemotrade, 99.8%).

VCD spectra were measured in the mid-IR region with a Fourier transform infrared spectrometer IFS-66/S (Bruker, Germany) equipped with the VCD/IRRAS module PMA 37 (Bruker, Germany) by the method described in detail elsewhere.[12] A low-pass filter (<1800 cm^{-1}), BaF$_2$ polarizer, ZnSe modulator (Hinds Instruments) oscillating at the frequency of 50 kHz and MCT (InfraRed Associates) detector were used. The noise spectra were calculated as a half of the difference between two VCD spectra obtained in two blocks of scans. Experimental VCD baselines were obtained for pure solvents. The IR absorption and VCD spectra were measured simultaneously both with a resolution of 8 cm^{-1} and a zero filling factor of 4. Samples were placed in a demountable cell A145 (Bruker, Germany) constructed of CaF$_2$ windows separated by a 0.1-mm Teflon spacer. The concentrations used were in the range of 0.05−0.11 mol L^{-1}.
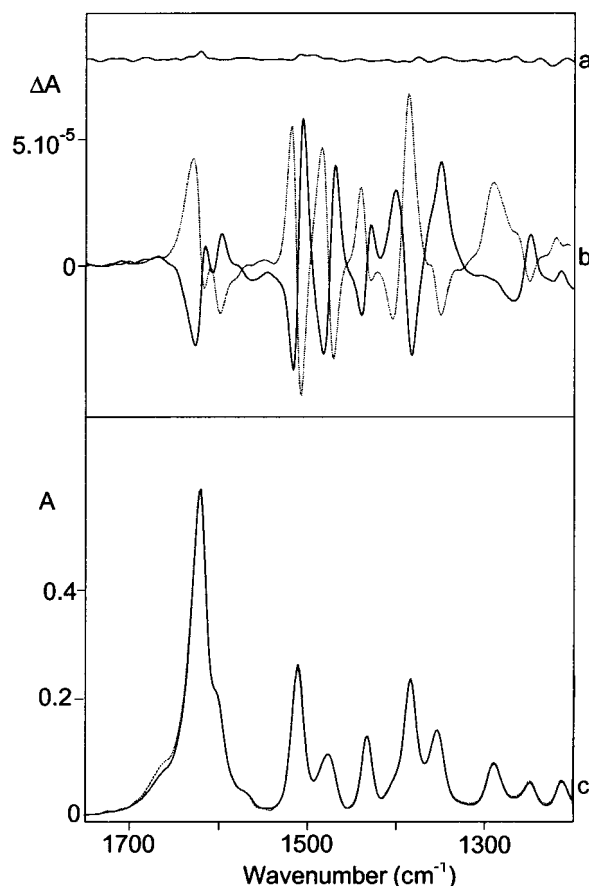

Figure 1. VCD (b), absorption (c), and noise VCD (a) spectra of 1,1′-binaphthyl-2,2′-diamine in DMSO-d_6 for the (S)- (full line) and (R)-(dashed line) enantiomers.

Calculations

Computations were performed for individual molecules in a vacuum. Trial computations implementing the conductor-like screening continuum solvent model[13] did not provide convincing improvement of the spectra and are not shown here. As follows from general experience, however, the rather minor effect of the solvent on VCD intensities can be expected. Program Gaussian[14] was used for the calculations performed at the facilities of the Institute of Chemical Technology and the Academy of Sciences. Geometry of each binaphthyl derivative was optimized by the energy minimization, then harmonic vibrational frequencies and VCD intensities were computed. Theoretical spectra were simulated by using Lorentzian bands with a bandwidth of 5 cm^{-1}, approximately matching the observed broadening. The calculations were performed with the BPW91 density functional[15] using the 6-31G** basis set with default parameters of Gaussian. The HF/4-31G level was used for estimation of starting geometries. Previously, the BPW91 functional provided faithful simulations of VCD spectra for similar molecules.[16] Other functionals (HF, B3LYP, MPW1PW91) gave inferior results in test calculations for our systems. Stephens' magnetic field perturbation theory with the gauge-independent atomic orbitals[17] implemented in Gaussian was used for the computation of the atomic axial tensor.

Results and Discussion

Experimental Accuracy. VCD and IR absorption spectra were measured for both enantiomers of all the compounds **2**−**7**. As a typical example we show spectra of (S)- and (R)-1,1′-binaphthyl-2,2′-diamine (**3**) measured in DMSO-d_6 in Figure 1
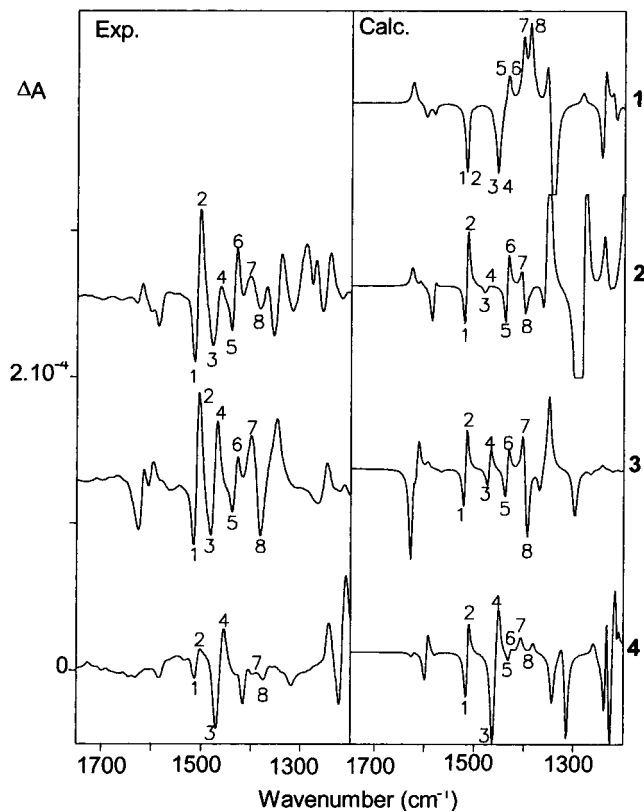
VCD of 1,1′-Binaphthyl Derivatives

J. Phys. Chem. A, Vol. 105, No. 39, 2001 **8933**

Figure 2. Experimental (left) and simulated (right) VCD spectra of the symmetrical (R$_2$=H) (S)-binaphthyl derivatives **1**−**4**.

Figure 3. Experimental (left) and simulated (right) VCD spectra of the R$_2$-substituted derivatives **5** (top) and **6** (bottom), for (S)-enantiomers.

to demonstrate the quality of our data. Apparently, the selected wavelength region provides relatively rich spectra with well-resolved vibrational transitions. The (S)- and (R)-enantiomers provide almost identical absorption spectra, and their VCD spectra are nearly symmetrical with respect to the baseline. The noise spectrum demonstrates a favorable signal-to-noise ratio of the instrument, sufficient for reliable reproduction of the relative peak intensities.

The binaphthyls **1**−**7** can be roughly classified as symmetrical with the C_2 symmetry for structures **1**−**4** and **7** and nonsymmetrical (C_1) for compounds **5** and **6** substituted in position 3. The lowest-energy conformations possess a lower symmetry for **3** and **7** because of the rotation of the NH$_2$ and POH groups. Nevertheless, the two classes provide rather distinct VCD patterns. This is shown in Figures 2 and 3 where the experimental and calculated spectra of the symmetrical derivatives **2**−**4** and nonsymmetrical compounds **5** and **6** are plotted, respectively. For simplicity, only spectra of (S)-enantiomers are shown. The quality of the mirror symmetry of the spectra with the (R)-enantiomers is similar to that shown in Figure 1 for **3**. As mentioned above, experimental VCD could not be obtained for the parent binaphthyl **1**. Nevertheless, we found it useful to include it as the basic system in our series, because it makes understanding and interpretation of measured VCD intensities easier.

Excellent agreement in positions, signs, and relative intensities of VCD bands for the experimental and calculated spectra can be seen. Several experimental VCD and absorption bands can be directly linked to the calculations, as indicated in Figures 2 and 3, and more vibrational modes can be assigned by a combined analysis of the VCD and absorption bands (Tables 2 and 3). The nature of corresponding normal modes was determined by a dynamic visualization of the normal mode displacements. In addition, the modes were assigned to indi-
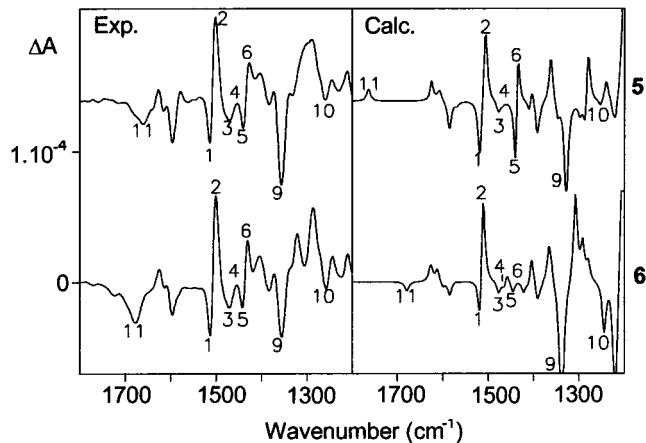
vidual groups of atoms by using the calculated distribution of vibrational kinetic energy. Contributions of particular molecular parts could thus be examined. However, we do not list complete mode assignments and analyses here, because these data are useless given the resolution of the condensed-phase spectra, and can be easily reproduced with commercially available software. Instead, we emphasize spectral features important for structural analysis.

C2 Symmetrical Compounds. As seen in Figure 2, bands 1−8 are common for all derivatives in experimental as well as calculated spectra. This region is dominated by the vibrations of the binaphthyl core, typically resulting in splitting bands because of the C_2 symmetry and the dipolar exciton coupling of the naphthyl chromophores. For example, two normal modes with opposite signs of VCD intensities in parent binaphthyl **1** result in a negative VCD band located at 1517 cm^{-1} (bands 1 and 2 in Figure 2). These modes can be identified for the derivatives **2**, **3**, and **4** as more conservative doublets localized at 1521−1513 cm^{-1} in simulated VCD spectra and corresponding bisignate doublets found experimentally at 1516−1502 cm^{-1}. The vibrations responsible for bands 1 and 2 are localized around atoms C$_6$, C$_{6'}$, C$_7$, and C$_{7'}$ in the binaphthyl core and consist mainly of C−C stretchings and C−H bendings.

Similarly, modes 5 and 6 result in the positive band calculated at 1438 cm^{-1} for parent binaphthyl **1** and correspond to positive doublets 1439−1428 cm^{-1} in calculated spectra of the derivatives **2**, **3**, and **4**. These can be easily identified in experiments for **2** and **3** from 1440 to 1428 cm^{-1}. In the experimental spectrum of **4** (left-hand side, Figure 2), the doublet 5, 6 is overlapped with vibrations of the sulfonate group. The modes 5, 6 are predominantly localized in the vicinity of atoms C$_6$, C$_{6'}$, C$_9$, C$_{9'}$, and H$_9$, H$_{9'}$.

The intensities of modes 7 and 8 were both calculated positive for parent binaphthyl **1**, whereas for derivatives **2**, **3**, and **4** negative doublets were located in calculated and experimental spectra at 1405−1385 cm^{-1}. Atoms C$_8$, C$_{8'}$, H$_8$, H$_{8'}$, and C$_4$, C$_{4'}$ contribute mostly to the energy of these vibrations.

The parts of the molecule mostly vibrating in modes 1−2 and 5−8 are distant from positions 2, 2′ and thus do not interfere with modes involving the groups attached therein. On the other hand, bands 3 and 4 originate mainly in modes located close to the C$_2$ and C$_{2'}$ atoms. Clearly, a greater influence of the substituents on these modes is apparent both in the experimental and calculated spectra: The bands are red shifted and more intense in binaphthyl **4** in comparison with compounds **2** and **3**, cf. Figure 2. Note that in **4**, the substituent R$_1$ = SO$_3$CF$_3$ is

TABLE 2: Calculated Fundamental Frequencies (cm^{-1}) of the Binaphthyl Skeleton (1) and the Assignment to the Theoretical and Experimental Vibrations of the Derivative Compounds (2−7)

band	1(C$_2$) calc.	2(C$_2$) calc.	2(C$_2$) exp.	3(C$_1$) calc.	3(C$_1$) exp.	4(C$_2$) calc.	4(C$_2$) exp.	5(C$_1$) calc.	5(C$_1$) exp.	6(C$_1$) calc.	6(C$_1$) exp.	7(C$_1$) calc.	7(C$_1$) exp.
	1626 B	1628	**1619**	1627	**1628**	1624	**1622**	1626	**1624**	1628	**1625**	1625	**1624**
	1625 A	1628		1620		1625		1628		1626		1624	
	1600 B	1611		1597	**1599**	1595	**1585**	1608	**1597**	1600		1597	**1593**
	1598 A	1614		1595		1599		1614		1613		1595	
	1583 A	1587	**1586**	1570		1582		1586		1585	**1596**	1573	
	1581 B	1583		1567		1576		1569		1585		1581	
1	1517 A	1520	**1514**	1521	**1516**	1516	**1514**	1519	**1514**	1519	**1513**	1516	**1508**
2	1516 B	1517	**1504**	1518	**1505**	1513	**1503**	1506	**1501**	1512	**1500**	1517	
3	1463 A	1481	**1478**	1474	**1481**	1464	**1470**	1478	**1472**	1477	**1470**	1459	
4	1455 B	1473	**1464**	1469	**1467**	1453	**1454**	1469	**1453**	1464	**1454**	1455	**1467**
5	1439 B	1435	**1430**	1434	**1428**	1428		1439	**1440**	1445	**1442**	1431	
6	1435 A	1438	**1439**	1438	**1439**	1433		1436	**1428**	1437	**1430**	1431	**1437**
7	1405 A	1407	**1403**	1403	**1402**	1407	**1406**	1409	**1403**	1405	**1403**	1404	**1402**
8	1391 B	1400	**1383**	1394	**1384**	1385	**1394**	1392	**1384**	1392	**1384**	1390	**1380**
	1384 A	1390		1388		1384		1392				1383	
	1382 A	1385		1383		1385		1387		1386		1379	
	1356 B	1353	**1344**	1351	**1347**	1319	**1321**	1348		1362		1329	
9	1344 A	1363		1370		1345		1328	**1357**	1338	**1357**	1336	
10	1285 A	1292		1268		1261		1253	**1260**	1245	**1258**	1263	
	1246 B	1241	**1244**	1244	**1245**	1251		1240	**1242**			1249	
	1241 A	1277		1268		1261		1253		1230		1263	
	1222 B	1225		1223	**1216**	1224		1226		1225		1224	
	1220 A	1222		1224		1218	**1218**	1220		1220		1212	
	1196 B			1103									
	1172 A	1164		1206		1186				1158		1188	
	1157 B	1157		1157		1159		1158		1157		1159	
	1157 A	1156		1155		1160		1156		1155		1158	
	1149 B	1151		1153		1154		1165				1143	
	1145 A	1146		1152		1150		1149		1145		1142	

For each compound the symmetry of the conformer used for spectral simulation is given in parentheses. For **1** symmetries of the normal modes (A, B) are listed. Frequencies were calculated at the BPW91/6-31G** level. Numbered bands correspond to those in Figures 2−5.

TABLE 3: Side-Chain Vibrational Modes in the Binaphthyl Derivatives

compound/ group	mode	calculation	experiment, remark
2/OH	C−O torsion		mixed with almost all modes in measured range
	O−H bending	1164, 1199, 1295, 1351	also mixed with other modes; in regions with highest discrepancies between simulation and experiment
3/NH$_2$	NH bending	1613	1614, mixed with other modes, namely C−H bending, similarly as for OH bending
		1597, 1598	1596
		1299	1287
		1267	1262
	C−N stretch, NH wagging	1351	1346
4/OSO$_2$CF$_3$	S=O stretch	1317, 1326	1417, calculated frequency unrealistically low
	C−F stretch	1235, 1238	1240−1251
	S−C stretch	1214, 1218	1220; all OSO$_2$CF$_3$ modes rather localized, unlike for OH and NH$_2$ delocalized, similarly as in **2** and **3**
5,6/(OH)$_2$, COOH, COOCH$_3$	OH bend, C−O torsion		
	C=O stretch	1766, 1679	1678, hydrogen bonding lowers the frequency by about 90 cm^{-1}
	CH bend	1459−1473	minor contribution to IR and VCD spectra
7/PO$_4$H	P=O stretch	1288	1295, local mode
	C−O stretch	1212, 1197	1212−1220, mixed with binaphthyl modes

significantly heavier than in the other cases (R$_1$ = OH, NH$_2$) and is probably disturbing the naphthyl vibrations more. Also, an intensive repulsion supposedly exists between the bulky and polar groups in **4**.

VCD bands specific for different substituted groups R$_1$ can be identified in mid-IR region. For example, bands at 1630−1600 cm^{-1} in the experimental VCD of diamine **3** were assigned to the deformation vibrations of the C$_2$−NH$_2$ and C$_{2'}$−NH$_2$ groups and were calculated approximately at the same positions. Deformation vibrations of C$_2$−O−H and C$_{2'}$−O−H in both substituents R$_1$ in **2** result in VCD bands in the range of 1626−1586 cm^{-1} and 1620−1586 cm^{-1} in the simulated and experimental spectra, respectively.

Experimental bands at 1252−1242 cm^{-1} (calculated at 1238−1235 cm^{-1}) correspond to bending vibrations of the CF$_3$ group in **4**. Vibrations that involve S, O, and adjoining C$_2$ and C$_{2'}$ atoms in compound **4** are at 1330−1240 and 1417 cm^{-1} in calculated and experimental spectra, respectively. Such a large frequency error for vibrations of the sulfonate group is given by inadequate ab initio treatment of the sulfur atoms and perhaps by anharmonic effects, and could not be removed with our current computational means. Note, however, that unlike the frequencies, the IR and VCD intensity patterns are predicted faithfully also for these modes. Modes localized in the benzene rings connected by the 1−1′ bond contribute mainly to the bands at 1350−1400 cm^{-1}. As expected, they are more sensitive to

VCD of 1,1′-Binaphthyl Derivatives

J. Phys. Chem. A, Vol. 105, No. 39, 2001 **8935**

the substituents, as seen in Figure 2 in experimental and calculated VCD, as well as in the IR absorption in this region.

C1 Symmetry Compounds. Experimental and simulated VCD spectra of **5** and **6** are drawn in Figure 3. The signal-to-noise ratio, symmetry of VCD signals for (*S*)- and (*R*)-enantiomers, and coincidence of absorption spectra for both enantiomers were qualitatively the same as in Figure 1. Also, as apparent from Figure 3, main observed VCD features correspond nicely to the simulations.

Similar features can be found between the spectra of symmetrical and nonsymmetrical binaphthyls, as drawn in Figures 2 and 3, namely in the region of vibrations 1−8. In the symmetrical binaphthyls, doublets 1−2 and 5−6 are conservative in experimental and simulated spectra, whereas for the nonsymmetrical binaphthyls these couplets are positively biased. This can be explained by a perturbation of the C_2 symmetry and the exciton coupling between the two naphthyl chromophores. The doublets 1, 2 have negative and positive components at 1514−1519 cm^{-1} and 1500−1506 cm^{-1}, respectively, as found by both the experiment and the simulation. The negative lobe originates mainly from vibrations localized around atoms $C_{6'}$ and $C_{7'}$; i.e., on the naphthyl ring where the position 3 is not substituted. The positive part thus comes from vibrations around the C_6 and C_7 atoms on the substituted ring.

Bands 3 and 4 are least affected by the substitutions, because they are located (in experimental spectra, positive first) at 1470 cm^{-1} and 1453 cm^{-1} for all binaphthyls studied (calculated at 1478 and 1469−1472 cm^{-1}, respectively). In the nonsymmetrical binaphthyls, the negative component predominantly originates in vibrations of atoms $C_{2'}$, $C_{7'}$, and the hydrogen atom bonded to $C_{7'}$; the positive component comes predominantly from vibrations of atoms C_2, C_7 and from the C_2−H bending.

Other VCD bands in Figure 3 are not present in the spectra of symmetrical binaphthyls and stem from the carboxyl group. (i) A strong dominant negative band marked as 9 was observed at 1357 cm^{-1} and calculated at 1328 and 1338 cm^{-1} for **5** and **6**, respectively. This band was assigned to the deformation of the −C−O−H group. Vibration modes of this group contribute also with a much weaker VCD intensity to the bands at around 1298 cm^{-1}. (ii) A negative band marked as 10 in Figure 3 (located at 1260−1258 cm^{-1} and 1253−1245 cm^{-1} in experiment and calculation, respectively) was assigned to deformation vibrations of the COOH and CH$_3$ groups. (iii) The characteristic C=O stretching vibration (marked as 11) gives negative experimental bands for the (*S*)-enantiomer located at 1660 and 1678 cm^{-1} for **5** (R$_2$ = COOH) and **6** (R$_2$ = COOCH$_3$), respectively. The sign for **5** is not calculated correctly, probably because of the inadequate modeling of the hydrogen bonding. For the methylated compound, the correct VCD sign and better frequency were obtained by the simulation. The VCD signal of the CH$_3$ group is weak and overlapped by skeletal vibrations, and therefore cannot be clearly identified.

Fixation of the Naphthyl Planes Angle. Controlling the angle and hence its monitoring by VCD is important when supramolecular complexes based on the binaphthyl compounds are built. As a simplistic model of a well-defined system, experimental and simulated VCD spectra for both (*S*)- and (*R*)-enantiomers of the chain-bridged derivative **7** were measured and are plotted in Figure 4. A good agreement in the band positions and relative intensities between simulated and measured spectra can be observed, similarly as for the other systems.

Interesting differences between VCD of the chain-bridged derivative **7** and spectra of the flexible derivatives can be found. These will be documented on theoretical spectra of the parent
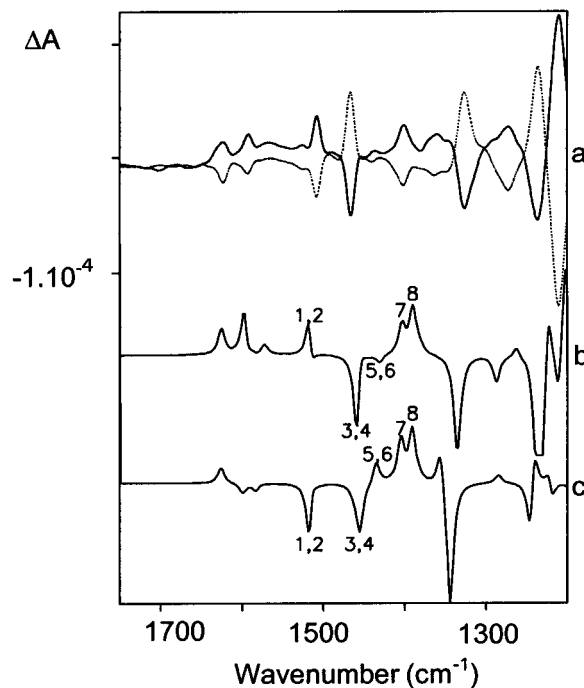

Figure 4. Experimental (a: (*S*)-, full line; (*R*)-, dashed line) and simulated (b: (*S*)-form) VCD spectra of 1,1′-binaphthyl-2,2′-diyl-hydrogenphosphate **7** and simulation for the parent (*S*)-binaphthyl **1** (c).

binaphthyl **1** because they describe experimental findings reasonably well. As mentioned above, bands 1 and 2 originate in vibrations around atoms C_6, $C_{6'}$, C_7, $C_{7'}$ both for **1** and **7**. However, in compound **7**, band 1 involves mainly vibrations of C_6, C_3, $C_{6'}$, $C_{3'}$, whereas band 2 involves mainly vibration of C_7, $C_{7'}$. Rotation strengths of both transitions 1 and 2 are both positive for **7**, but negative and positive for **1**, respectively. Bands 3 and 4 originate in vibrations of atoms close to substituents R$_1$ both in **1** and **7**. The signal of bands 5 and 6, originating in bending vibrations of C_5−H$_5$ and $C_{5'}$−H$_{5'}$, is positive in **1** but negative in **7**. Closer inspection reveals that in **7** atoms $C_{7'}$ and $C_{8'}$ participate more on these vibrations.

Coupled Oscillator Model. As indicated above, many spectral features can be explained on the basis of the simple coupled oscillator model.[19] The model was proposed for weakly interacting chromophores and is adequate for some modes of the naphthyl groups, as pointed out previously for C−H stretching.[6f] However, because the two groups are connected by the covalent bond and relatively close, their interaction cannot be restricted to dipole−dipole coupling.[10e,20] Thus, although VCD intensity of many modes primarily rises from this mechanism, sign and the resultant spectral pattern can be predicted reliably only by the ab initio simulation. For example, the modes numbered 1 and 2 (Figure 2) correspond to C−H bending vibration on the naphthyl residues. The coupled oscillator model predicts a conservative VCD couplet for the binaphthyl **1**, which is in a rough agreement with the ab initio computed rotational strengths for the symmetric (A, R= −17 × 10^{-8} Debye^2) and asymmetric (B, R = 13 × 10^{-8} Debye^2) mode. However, because of the small energy splitting of 1.0 cm^{-1} and a large band broadening, only a negative VCD signal appears in the spectrum. On the other hand, the splitting for these modes results in VCD couplets for the other compounds in Figure 2. This, as well as the intensity bias (positive, positive and negative for the compounds **2**, **3**, and **4**, respectively), is well reproduced by the ab initio calculation. The couplet signs of modes (1,2), (3,4), and (5,6) are equal for **2−4**,
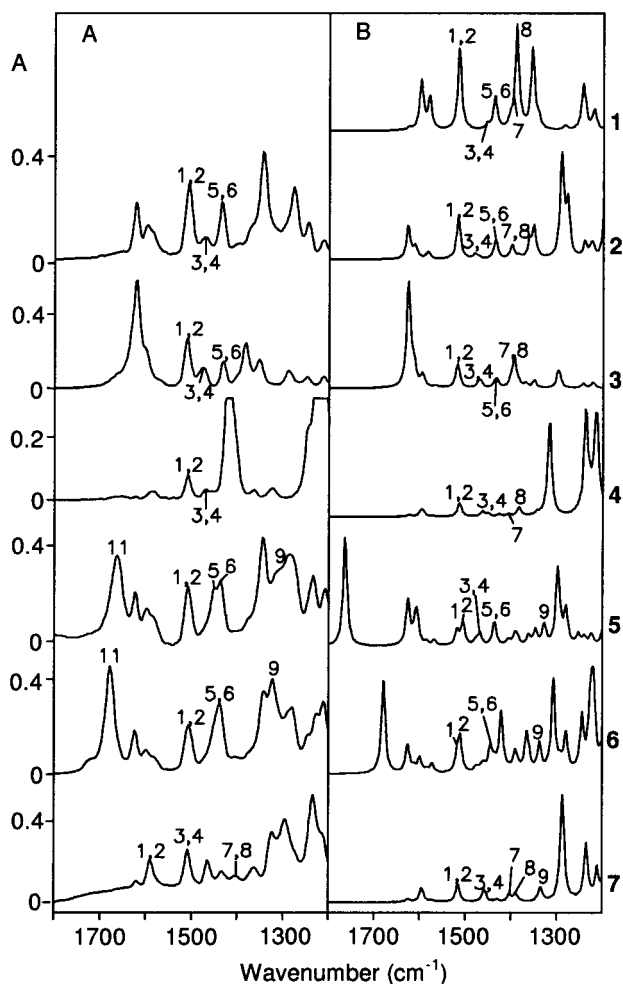
Figure 5. Experimental (left) and simulated (right) absorption spectra of binaphthyl derivatives **1**−**7**.

in accord with the coupled oscillator model dependent only on the juxtaposition of the binaphthyl planes, but the modes (7,8) provide an opposite couplet, which indicates a more complicated interaction between the two naphthyl groups than the dipole−dipole interaction.

Absorption Spectra. Experimental and simulated IR absorption spectra of the whole set are plotted in Figure 5. Similarly to VCD, skeleton bands 1−8 and bands specific for individual derivatives can be identified in IR. The transitions at 1622 cm^{-1} in experimental and 1626−1628 cm^{-1} in simulated spectra of **2** and **3** belong to deformation vibrations of C_2−OH, $C_{2'}$−OH, C_2−NH_2, and $C_{2'}$−NH_2 groups. The bands at 1240−1220 cm^{-1} both in experimental and simulated spectra of **4** originate from the deformation vibration involving atoms of the sulfonate group. The deformation vibrations of the −C−O−H group in substituents R_1 and R_2 of **5** and **6** cause the absorption signal near 1350 cm^{-1}, but the bands are superimposed and not resolved, similarly to corresponding VCD (band 9, Figure 3). The same can be said about the bending vibrations of −COOH and −COOCH₃ (band 10, Figure 3). The C=O stretching indicated by 11 in Figure 3 can be clearly distinguished in the absorption. Overall, it is apparent that structural features are reflected more in the VCD than in the absorption.

A direct link between normal modes of 1,1′-binaphthyl and those of the other derivatives can be obtained by comparison of calculated S-vectors, as summarized in Table 2. As a supplement to the visual inspection, numerical comparison was used based on the Cartesian tensor transfer techniques described

TABLE 4: Calculated Torsion Angles (deg) between the Two Naphthyl Planes

	compound						
angle	1	2	3	4	5	6	7
9′−1′−1−9	74	87	95	104	90	85	57
2′−1′−1−2	71	86	93	108	89	82	52

in ref 18. Similarity of the vibrational modes *i, j* was determined on the basis of the differences between corresponding *S*-vectors,

$$\delta = \Sigma_{\alpha,\lambda}(S^i_{\lambda\alpha} - S^j_{\lambda\alpha})^2 \qquad (1)$$

where the sum involves all coordinates α of all atoms λ. Best overlap was found for each atom in the two molecules before taking the differences of the vectors.

Clearly, most of the binaphthyl modes can be also found in the derivatives and the assignment agrees with the experimental positions (given in bold numbers in Table 2). In the first column, the band numbers correspond to those in Figures 2−5. Similarly, contribution of the side groups can be depicted, as described in detail above and summarized in Table 3. The vibrations of the substituents seem rather separated and independent from those of the binaphthyl core. This is in accord with the classical analytical concept of characteristic vibrations, unlike for strongly coupled aliphatic bicyclic systems in which absorption and VCD patterns could not be resolved into contributions from molecular parts.[21]

Geometry Consequences. Values of the angle θ as calculated for the lowest-energy conformers are listed in Table 4. These values, although obtained for single molecules in a vacuum, agree with those obtained by X-ray[5] and ECD studies,[6a−e] predicting the dihedral angle in the interval of 70−110°. A shallow torsional potential for this rotation allows a semifree movement of the binaphthyl rings in solution. Hydrogen bridging or attraction/repulsion of groups attached namely in the 2,2′ positions can partially restrict the motion. Although good models of solvent are not available for VCD, the agreement between experimental and calculated VCD spectra suggests that the influence of the solvent is rather limited. In **2**, **5**, **6**, where R_1 = OH, the dihedral angle θ is in the interval 82−89°. Compound **4,** with the large substituent R_1 = OSO_2CF_3, adopts a conformation with a higher value of θ, 104−107°. This can be understood by a steric and electrostatic repulsion of the −OSO_2CF_3 groups. Geometry with smaller dihedral angles was found for parent (**1**, 70−74°) and PO_4H-bridged (**7**, 52−57°) binaphthyl. For the derivatives **1**−**6** a smaller angle of about 60°is sterically possible and in many cases can be stabilized by internal hydrogen bridges, but we can exclude an occurrence of this conformation on the basis of the VCD spectra. Probably only a strong covalent bond, such as in compound **7**, can force such a deviation of the naphthyl rings from orthogonality. Two or more solvent-oriented hydrogen bonds are apparently preferred as energetically more convenient for the 2,2′-derivatives.

Unfortunately, the interaction of the flexible polar groups forming hydrogen bridges with the solvent could not be modeled in detail. Thus, preferred conformation of the OH, COOH, and COOCH₃ groups could not be assessed reliably. Nevertheless, as shown above, the structures obtained by vacuum minimization well explain measured data, and the hydrogen bonding affects only a few spectral features, such as the frequency of the C=O stretching group. Also, the VCD technique is in principle able to monitor the structure of all molecular parts, providing that an adequate theoretical model is available. Thus these challenges should stimulate further development of VCD instrumentation as well as the quantum chemical tools.
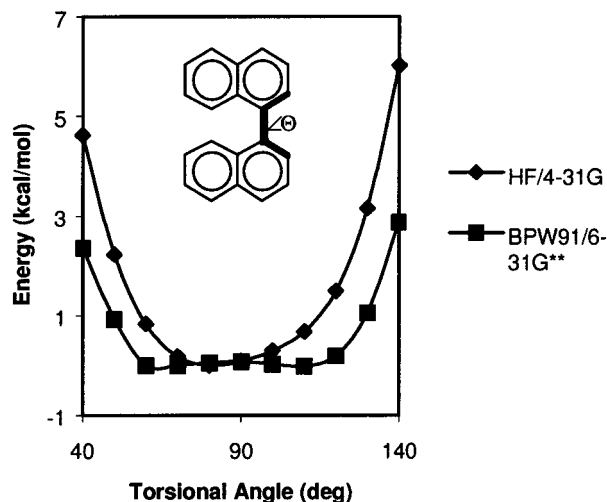
VCD of 1,1′-Binaphthyl Derivatives

J. Phys. Chem. A, Vol. 105, No. 39, 2001 **8937**

Figure 6. Calculated energies of 1,1′-binaphthyl conformers. Relative energies with respect to the minima of the potential wells are plotted as obtained at the HF/4-31G and BPW91/6-31G** levels for 11 torsion angles θ. All other geometry parameters were optimized by energy minimization for each point.
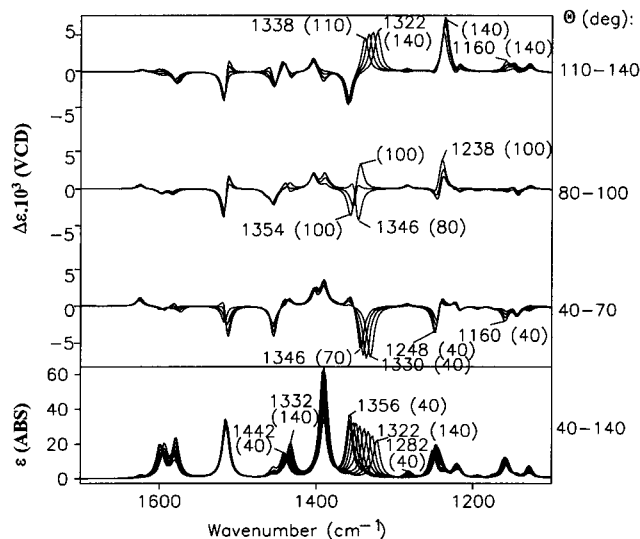

Figure 7. Simulated dependence of (*S*)-1,1′-binaphthyl VCD and absorption spectra on the torsion angle. Frequencies and corresponding values of θ (in parentheses) are indicated for peaks most sensitive to the conformation.

Sensitivity of the 1,1′-Binaphthyl Spectra to the Conformation. To estimate the sensitivity of absorption and VCD spectra to the changes of the angle θ we simulated the spectra for 11 conformers of 1,1′-binaphthyl. Relative energies of the conformers were obtained at the HF/4-31G and BPW91/6-31G** levels and are plotted in Figure 6. Clearly the changes around the perpendicular arrangement ($\theta = 90°$) are quite small if compared with the Boltzmann quantum at the room temperature (0.6 kcal/mol), and the BPW91 method even provides a shallow double-well potential. The flexibility is in accord with the broad range of the angles predicted for the derivatives and given in Table 4.

The conformers, however, give distinct VCD spectra as seen from the simulations (at the BPW91/6-31G** level) in Figure 7. The spectra are grouped into three plots in the upper part of the figure so that the changes can be seen better. The (+/−) couplet around 1516 cm^{-1} for $\theta = 40°$ becomes a negative VCD signal for the values of θ between 50 and 70° and finally changes its sign (−/+) for $\theta > 80°$. This is in agreement with

our analysis (cf. peaks labeled 1,2 in Figures 2−5), because the derivatives **2**−**6** with $\theta > 80°$ (see Table 4) exhibit the (−/+) pattern, whereas derivative **7** with θ 55° gives a negative signal (experimentally at 1508 cm^{-1}). Similarly, small values of θ favor a negative VCD around 1460 cm^{-1} in Figure 7, in agreement with the experiment for **7** (transitions 3,4 in Figure 4). The region 1320−1370 cm^{-1} is most affected by the changes of the angle, and the biggest changes in VCD take place around θ 90°. This is qualitatively in agreement with the rich features that appear in the experimental spectra of the derivatives. Unfortunately, the signal of the binaphthyl core is overlapped with that from the functional group in this region, which makes the analysis difficult.

The absorption spectra (lower part, Figure 7) are clearly less sensitive to the conformation, with the exception of the region 1320−1370 cm^{-1}. The absorption in this region is caused by a delocalized mode composed of C−H bending and a deformation of the binaphthyl ring in the vicinity of the σ C−C bond. Typically, a modest monotonic dependence of the frequencies and intensities on θ can be seen for the other absorption peaks in Figure 7. This corresponds to the small changes observed for the set of the derivatives (Figure 5, Table 2) for binaphthyl modes uncoupled to the functional groups.

Conclusions

A very good agreement between experimental and simulated VCD and absorption IR spectra was achieved. A band-to-band correspondence enabled us to assign most of the fundamental transitions and determine how various parts of the binaphthyl derivatives contribute to the VCD signal in the mid-IR region. Identification and assignment of vibration modes in VCD spectra is easier and more straightforward than in the IR absorption spectra. Moreover, conformational information can be obtained on the basis of comparison of the simulated and measured VCD spectra. Skeletal vibrations of the binaphthyl core dominated were clearly distinguished from those originating at the substituents at positions 2, 2′, and 3. Binaphthyl conformation determined by VCD in solution is consistent with the results obtained for liquid and solid state by X-ray and ECD techniques. Sensitivity of the VCD spectroscopy to binaphthyl structure and conformation can be used in future monitoring of such systems in chiral studies of molecular recognition and chiral synthesis.

References and Notes

(1) (a) Marchand, A. P.; Chong, H.-S.; Ganguly, B. *Tetrahedron: Asymmetry* **1999**, *10*, 4695. (b) Wan, K. T.; Davis, M. E. *Nature* **1994**, *370*, 449.

(2) Pu, L. *Chem. Rev.* **1998**, *98*, 2405.

(3) Kavenová, I.; Holakovský, R.; Hovorka, M.; Kříž, V.; Anzenbacher, P. Jr.; Matějka, P.; Král, V.; Genge, J. W.; Sessler, J. L. *Chem. Listy* **1998**, *92*, 147.

(4) (a) Hayashi, T.; Kawatsura, M.; Uozumi, Y. *Chem. Commun.* **1997**, 561. (b) Tenaglia, A.; Heumann, A. *Angew. Chem., Int. Ed. Engl.* **1999**, *38*, 2180. (c) Nakamura, H.; Nakamura, K.; Yamamoto, Y. *J. Am. Chem. Soc.* **1998**, *120*, 4242. (d) Kubo, Y. *Synlett* **1999**, *2*, 161. (e) Rusin, O.; Král, V. *Chem. Commun.* **1999**, 2367. (f) Furutani, T.; Hatsuda, M.; Imashiro, R.; Seki, M. *Tetrahedron: Asymmetry* **1999**, *10*, 4763. (g) Ishii,

8938 *J. Phys. Chem. A, Vol. 105, No. 39, 2001*

Setnička et al.

A.; Soloshonok, V. A.; Mikami, K. *J. Org. Chem.* **2000**, *65*, 1597. (h) Mikami, K.; Matsukawa, S.; Kyaki, Y.; Ikariya, T. *Tetrahedron Lett.* **2000**, *41*, 1931. (i) Rao, V. D.; Periasamy, M. *Tetrahedron: Asymmetry* **2000**, *11*, 1151. (j) Hodgson, D. M.; Stupple, P. A.; Johnstone, C. *Chem. Commun.* **1999**, 2185. (k) Yang, X.-W.; Sheng, C.-H.; Wang, H.-S.; Su, W.; Wang, R.; Chan, A. S. C. *J. Org. Chem.* **2000**, *65*, 295.

(5) (a) Kuroda, R.; Mason, S. F. *J. Chem. Soc., Perkin Trans. 2* **1981**, 167. (b) Kress, R. B.; Duesler, E. N.; Etter, M. C.; Paul, I. C.; Curtin, D. Y. *J. Am. Chem. Soc.* **1980**, *102*, 7709. (c) Akimoto, H.; Shioiri, T.; Iitaka, Y.; Yamada, S.-I. *Tetrahedron Lett.* **1968**, *1*, 97.

(6) (a) Mason, S. F.; Seal, R. H.; Roberts, D. R. *Tetrahedron* **1974**, *30*, 1671. (b) Di Bari, L.; Pescitelli, G.; Salvadori, P. *J. Am. Chem. Soc.* **1999**, *121*, 7998. (c) Di Bari, L.; Pescitelli, G.; Marchetti, F.; Salvadori, P. *J. Am. Chem. Soc.* **2000**, *122*, 6395. (d) Rosini, C.; Superchi, S.; Peerlings, H. W. I.; Meijer, E. W. *Eur. J. Org. Chem.* **2000**, 61. (e) Nehira, T.; Parish, C. A.; Jockusch, S.; Turro, N. J.; Nakanishi, K.; Berova, N. *J. Am. Chem. Soc.* **1999**, *121*, 8681. (f) Nakao, K.; Kyogoku, Y.; Sugeta, H. *Faraday Discuss.* **1994**, *99*, 77.

(7) (a) Proni G.; Spada G. P. *J. Org. Chem.* **2000**, *65*, 5522. (b) Gottarelli, G.; Hibert, M.; Samori, B.; Solladie, G.; Spada, G. P.; Zimmermann, R. *J. Am. Chem. Soc.* **1983**, *105*, 7318. (c) Gottarelli, G.; Spada, G. P.; Bartsch, R.; Solladie, G.; Zimmermann, R. *J. Org. Chem.* **1986**, *51*, 589. (d) Naciri, J.; Spada, G. P.; Gottarelli, G.; Weiss, R. G. *J. Am. Chem. Soc.* **1987**, *109*, 4352.

(8) (a) Mikami, K.; Motoyama, Y.; Terada, M. *Inorg. Chim. Acta* **1994**, *222*, 71. (b) Harada, T.; Takeuchi, M.; Hatsuda, M.; Ueda, S.; Oku, A. *Tetrahedron: Asymmetry* **1996**, *7*, 2479. (c) Lustenberger, P.; Martinbor-ough, E.; Denti T. M.; Diederich, F. *J. Chem. Soc., Perkin Trans. 2* **1998**, 747.

(9) Kranz, M.; Clark, T.; Schleyer, P. von R. *J. Org. Chem.* **1993**, *58*, 3317.

(10) For reviews, see (a) Keiderling, T. A. In *Practical Fourier Transform Infrared Spectroscopy. Industrial and Laboratory Chemical Analysis*; Ferraro, J. H.; Krishnan, K., Eds.; Academic: San Diego, 1990; pp 203−284. (b) Nafie, L. A. *Appl. Spectrosc.* **1996**, *50*, 14A. (c) Polavarapu, P. L.; Zhao, C. *Fresenius' J. Anal. Chem.* **2000**, *366*, 727. (d)

Barron, L. D. In *Molecular Light Scattering and Optical Activity;* Cambridge University Press: Cambridge, U.K., 1982. (e) Bouř, P.; Keiderling, T. A. *J. Am. Chem. Soc.* **1992**, *114*, 9100.

(11) (a) Hovorka, M.; Smíšková, I.; Holakovský, R.; Beran, J.; Stibor, I. *Pure Appl. Chem.* **1998**, *70*, 415. (b) Sudo, Y.; Yamaguchi, T.; Shinbo, T. *J. Chromatogr. A* **1998**, *813*, 35. (c) Lellek, V.; Stibor, I. *Collect. Czech. Chem. Commun.* **1997**, *62*, 925.

(12) Urbanová, M.; Setnička, V.; Volka, K. *Chirality* **2000**, *12*, 199.

(13) Klamt, A. *J. Phys. Chem.* **1995**, *99*, 2224.

(14) Frisch, M. J.; Trucks, G. W.; Schlegel, H. B.; Scuseria, G. E.; Robb, M. A.; Cheeseman, J. R.; Zakrzewski, V. G.; Montgomery, J. A.; Stratmann, R. E.; Burant, J. C.; Dapprich, S.; Millam, J. M.; Daniels, A. D.; Kudin, K. N.; Strain, M. C.; Farkas, O.; Tomasi, J.; Barone, V.; Cossi, M.; Cammi, R.; Mennucci, B.; Pomelli, C.; Adamo, C.; Clifford, S.; Ochterski, J.; Petersson, G. A.; Ayala, P. Y.; Cui, Q.; Morokuma, K.; Malick, D. K.; Rabuck, A. D.; Raghavachari, K.; Foresman, J. B.; Cioslowski, J.; Ortiz, J. V.; Stefanov, B. B.; Liu, G.; Liashenko, A.; Piskorz, P.; Komaroni, I.; Gomperts, R.; Martin, R. L.; Fox, D. J.; Keith, T.; Al-Laham, M. A.; Peng, C. Y.; Nanayakkara, A.; Gonzales, C.; Challacombe, M.; Gill, P. M. W.; Johnson, B. G.; Chen, W.; Wong, M. W.; Andres, J. L.; Head-Gordon, M.; Replogle, E. S.; Pople, J. A. *Gaussian 98,* revisions A.3 and A.7; Gaussian, Inc.: Pittsburgh, PA, 1998.

(15) (a) Becke, A. D. *Phys. Rev. A* **1988**, *38*, 3098−3100. (b) Perdew, J. P.; Wang, Y. *Phys. Rev. B* **1992**, *45*, 13244.

(16) (a) Bouř, P.; Záruba, K.; Urbanová, M.; Setnička, V.; Matějka, P.; Fiedler, Z.; Král, V.; Volka, K. *Chirality* **2000**, *12*, 191. (b) Bouř, P.; McCann, J.; Wieser, H. *J. Phys. Chem. A* **1998**, *102*, 102. (c) Bouř, P.; McCann, J.; Wieser, H. *J. Phys. Chem. A* **1997**, *101*, 9783.

(17) Devlin, F. J.; Stephens, P. J.; Cheeseman, J. R.; Frisch, M. J. *J. Phys. Chem. A* **1997**, *101*, 9912.

(18) Bouř, P.; Sopková, J.; Bednárová, L.; Maloň, P.; Keiderling, T. A. *J. Comput. Chem.* **1997**, *18*, 646.

(19) Holzwarth, G.; Chabay, I. *J. Chem. Phys.* **1972**, *57*, 1632.

(20) Bouř, P.; Keiderling, T. A. *J. Am. Chem. Soc.* **1993**, *15*, 9602.

(21) Rauk, A.; McCann, J. L.; Wieser, H.; Bouř, P.; El'natanov, Y. I.; Kostyanovsky, R. G. *Can. J. Chem.* **1998**, *76*, 717.